frontiers | Frontiers in Carbon

TYPE Original Research
PUBLISHED 13 December 2023
DOI 10.3389/frcrb.2023.1300811

OPEN ACCESS

EDITED BY
Marinella Striccoli,
Consiglio Nazionale delle Ricerche—CNR, Italy

REVIEWED BY
Octavian Buiu,
National R&D Institute for Microtechnologies-IMT Bucharest, Romania
Gianluca Minervini,
Politecnico di Bari, Italy

*CORRESPONDENCE
Cintya. D. A. E. S. Barbosa,
cintya.barbosa@iqb.ufal.br

RECEIVED 23 September 2023
ACCEPTED 22 November 2023
PUBLISHED 13 December 2023

CITATION
Da Silva LE, Araujo APdL, Almeida JH, de Vasconcelos LBOD, Silva MdO, Lima DJP, Viana RdS, Ferro JNdS, Goulart MOF, Xavier JA and Barbosa CDAES (2023), Carbon dots-based fluorescent films to act as a potential antioxidant agent and pH ratiometric sensor for skin applications.
Front. Carbon 2:1300811.
doi: 10.3389/frcrb.2023.1300811

Carbon dots-based fluorescent films to act as a potential antioxidant agent and pH ratiometric sensor for skin applications

Livia E. Da Silva[1], Anna Paula de L. Araujo[1], James Henrique Almeida[2], Ledja. B. O. D. de Vasconcelos[1], Messias de O. Silva[1], Dimas. J. P. Lima[1], Rodrigo da S. Viana[3], Jamylle N. de S. Ferro[2], Marília O. F. Goulart[1], Jadriane A. Xavier[1] and Cintya. D. A. E. S. Barbosa[1]*

[1]Institute of Chemistry and Biotechnology, Federal University of Alagoas, Maceió, Alagoas, Brazil, [2]Institute of Biological Sciences and Health, Federal University of Alagoas, Maceió, Alagoas, Brazil, [3]Technology Center, Federal University of Alagoas, Maceió, Alagoas, Brazil

The wound healing process is accompanied by changes in pH values. Monitoring this physicochemical parameter can indicate the effectiveness of the applied treatment and act as early identification of wound infection. This study focuses on the development of a fluorescent film-based polyvinyl alcohol (PVA) and carbon dots (CDs) derived from lemon bagasse (CD-L) and *ortho*-phenylenediamine (CD-oPD) named to act as antioxidants and potential ratiometric fluorescent pH sensors, in wound applications. The I_{460}/I_{550} intensity ratio, as a function of pH value for the dual-system CDs prepared from the mixture of CD-L and CD-oPD, named CD-L/oPD, was investigated. The fit corresponded to a sigmoidal function in the pH range of 5–10, with a relationship having a r^2 = 0.992. The variation in the values of the I_{460}/I_{550} ratio allows for the visualization of the color change from yellowish-green to green with increasing pH. Through a simulated *ex vivo* pig skin model, it was possible to note that the films prepared from mixed of the CD-L and CD-oPD carbon dots incorporated in a matrix PVA named CD-L/oPD-F was more efficient at visually discriminating color in relation to changes in pH than the films prepared from both individual CD-L (CD-L-F) and CD-oPD (CD-oPD-F) carbon dots. CD-L and CD-oPD demonstrated antioxidant capacity against reactive oxygen species (ROS). The IC_{50} values for CD-L and CD-oPD were 56.7 and 39.5 μg mL^{-1} in the DPPH$^{\bullet}$ inhibition assay, and 25.1 and 63.4 μg mL^{-1} in the HOCl scavenging one, respectively. MTT viability assays using human non-tumoral skin fibroblast (HFF-1) cell showed a cell survival rate of over 80% for both CDs up to a concentration of 1,000 μg mL^{-1}. Finally, the developed films can act in a bifunctional way, by monitoring healing through pH changes and by acting as an antioxidant agent in the treatment of wounds.

KEYWORDS

carbon dots, wound healing, ROS scavenger, polyvinyl alcohol, PH sensor film, dual emission

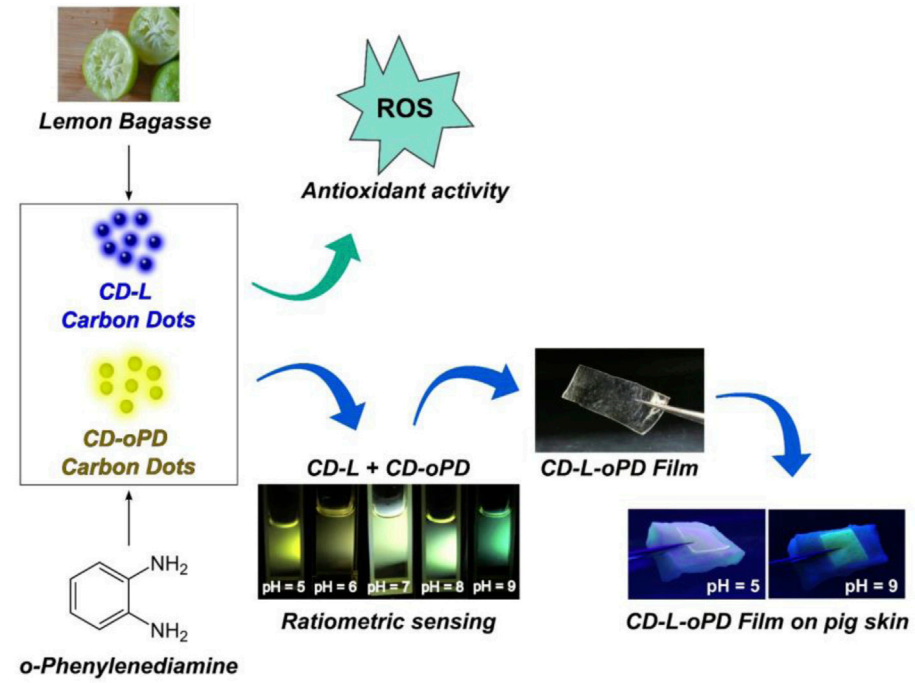

GRAPHICAL ABSTRACT

1 Introduction

Carbon dots are luminescent carbon nanoparticles (CNP) with sizes smaller than 10 nm and a spherical morphology (He et al., 2022; Wang et al., 2022). A graphitic structure forms the core, while the surface contains functional groups characteristic of the materials used during synthesis, mainly from the precursor (Ding et al., 2020; He et al., 2022; Davi, L. B. O. et al., 2021). CDs exhibit excellent optical properties, such as fluorescence in the visible spectrum, good dispersion in water, biocompatibility, photo-stability, low toxicity, antimicrobial activity, and low-cost synthesis (Mary et al., 2022). These properties associated with their non-invasiveness and good sensitivity have contributed to the development of various biological fluorescent sensors (Omidi et al., 2017; Yang et al., 2019).

The pH in biological systems plays a critical role in maintaining homeostasis and regulating vital processes (Mei et al., 2022). In this sense, a number of diseases are associated with disrupted pH values, and monitoring their changes is important to aid treatment. (Xia et al., 2019; Macairan et al., 2020). The exudates (liquids) released in the wounds during the healing process are capable of responding to pH, since the pH value influences physiological processes, such as the inflammatory response, collagen formation and angiogenesis (Zhu et al., 2020). The skin surface has a typical pH value ranging from 4 to 6, providing resistance against microbial invasion (Zhu et al., 2020; Sharma et al., 2023). However, chronic wounds have a more alkaline pH, between 7 and 9, and are more vulnerable to bacterial infections, while acute wounds have a pH similar to that of the skin under normal conditions, around 4 to 6, due to the activity of neutrophils which prevent the colonization of bacteria (Kadam et al., 2019; Zhu et al., 2020; Pang et al., 2023). In this sense, pH can help monitoring wound healing by enabling previous information to be provided which can contribute to effective treatment (Tang et al., 2021).

CDs have emerged as versatile and promising materials in the field of pH sensing. When exposed to different pH environments, CDs exhibit alterations in their emission spectra, resulting in changes in the wavelength of the emission or intensity (Yang et al., 2019; Zhang et al., 2019; Ehtesabi et al., 2020; Liu et al., 2021). pH-responsive property has positioned them as valuable tools for pH-sensing applications in various systems (Wang et al., 2020; Cui et al., 2021). Although studies on the treatment of wounds using CDs are in progress, the use of these nanoparticles in the detection of pH in wounds is rare (Omidi et al., 2017; Kasouni et al., 2021; Wu et al., 2022; Farshidfar et al., 2023). Omidi et al. (2017) synthesized single-channel CDs with blue emission derived from ammonium citrate to fabricate CD/chitosan nanocomposite films for application in wound healing. The results had shown that they were able to detect pH variation, during *in vivo* stages of wound healing (rat model). Yang et al. (2019) also prepared orange-emitting CDs using 1, 2, 4-triaminobenzene and urea (O-CDs), applied in the monitoring of wound healing, through the detection of pH values variation. Medical cotton cloth (MCC) was used as a support for the O-CDs and the combined (O-CDs/MCC) system was responsive to a pH range of 5 up 9.

However, the presence of only one emission band and/or gradation of wavelength of the maximum emission changes with low clarity, and difficulties to be visualized challenged the pH detection. In light of the limitations of single-channel nanoparticles, researchers are developing ratiometric sensors to improve the sensitivity of CDs to pH. (Song et al., 2017; Lei et al., 2020; Xu et al., 2020; Li et al., 2021; Silva et al., 2022). Ratiometric fluorescent sensors typically exhibit dual emission

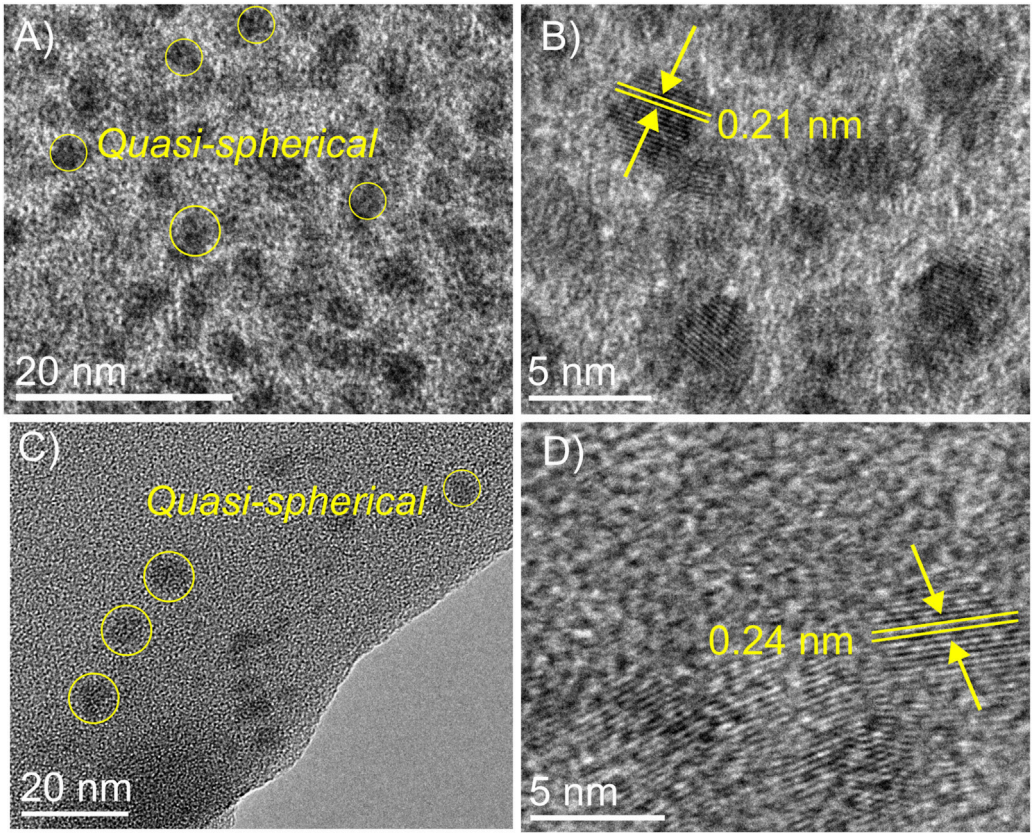

FIGURE 1
TEM micrographs for CD-L **(A,B)** and CD-oPD **(C,D)**.

bands at different wavelengths (Silva et al., 2022). A correlation is provided from the ratios of the fluorescence intensities of the different wavelengths of the sample, which minimizes background interferences, improving the sensitivity, precision and detection of the material (Li et al., 2021). In addition, ratiometric sensors enable rapid detection due to the response of the sample, which can also be seen with the naked eye. From this perspective, they can be applied to the detection of ions, pH, temperature, diseases, etc (Lei et al., 2020; Xu et al., 2020; Li et al., 2021). The advantages of these sensors, combined with the unique properties of CDs, allow the development of new platforms for *in situ* pH detection in biological systems with high efficiency. In this regard, the obtained results are highly promising for early diagnosis, and treatment's monitoring of diseases, such as chronic wounds (Yang et al., 2019; Farshidfar et al., 2023; Sharma et al., 2023).

Additionally, the use of CDs as antioxidant agents for therapeutic applications has been widely explored, however, in wounds, are still not common (Huangfu et al., 2021; Moniruzzaman et al., 2022; Roy et al., 2022; Varillas et al., 2022). In this sense, Qu et al. (2023) synthesized positively charged CDs from *p*-phenylenediamine and polyethyleneimine and studied their ability to reduce radicals as $DPPH^{\bullet}$, $^{\bullet}OH$ and $O_2^{\bullet-}$ in wounds, and results indicated that CDs effectively eliminated excess of these radicals, and relieved excessive inflammatory responses (Qu et al., 2023). Reactive oxygen species (ROS) are formed during normal cellular respiration, but studies have shown that in excess they can contribute to the development and progression of diseases resulting from oxidative stress (Juan et al., 2021; Dong et al., 2022). According to the intensity scale, we have the so-called physiological oxidative stress (eustress), essential for redox signaling and excessive and toxic oxidative stress, which causes damage to biomolecules (distress) (Sies et al., 2017). In general, wounds healing experiences three phases: inflammation, proliferation and maturation. In the inflammatory phase, an excess of ROS is produced, which is considered to be the main factor hindering skin regeneration (Bankoti et al., 2017). Thus, distress occurs, causing oxidative structural modifications in lipids, DNA, and proteins, leading to necrosis at the wound site (Bankoti et al., 2017; Juan et al., 2021).

The immobilization of CDs-based colorimetric/fluorescent pH sensors, and antioxidant agents in polymeric matrices is a good strategy for their use as bioactive dressings (Liu et al., 2021). In this sense, due to its properties of biocompatibility, hydrophilicity, low cost, and known benefits in wound healing, the synthetic polyvinyl alcohol (PVA) has been explored in the manufacture of dressings, usually associated with other organic and inorganic compounds (Moghaddam et al., 2021; Jin, 2022; Qu et al., 2023).

As such, this study aims to develop biocompatible, antioxidant fluorescent pH sensors using dual-system CDs prepared from lemon peel bagasse (CD-L) and *o*-phenylenediamine (CD-oPD) to offer a

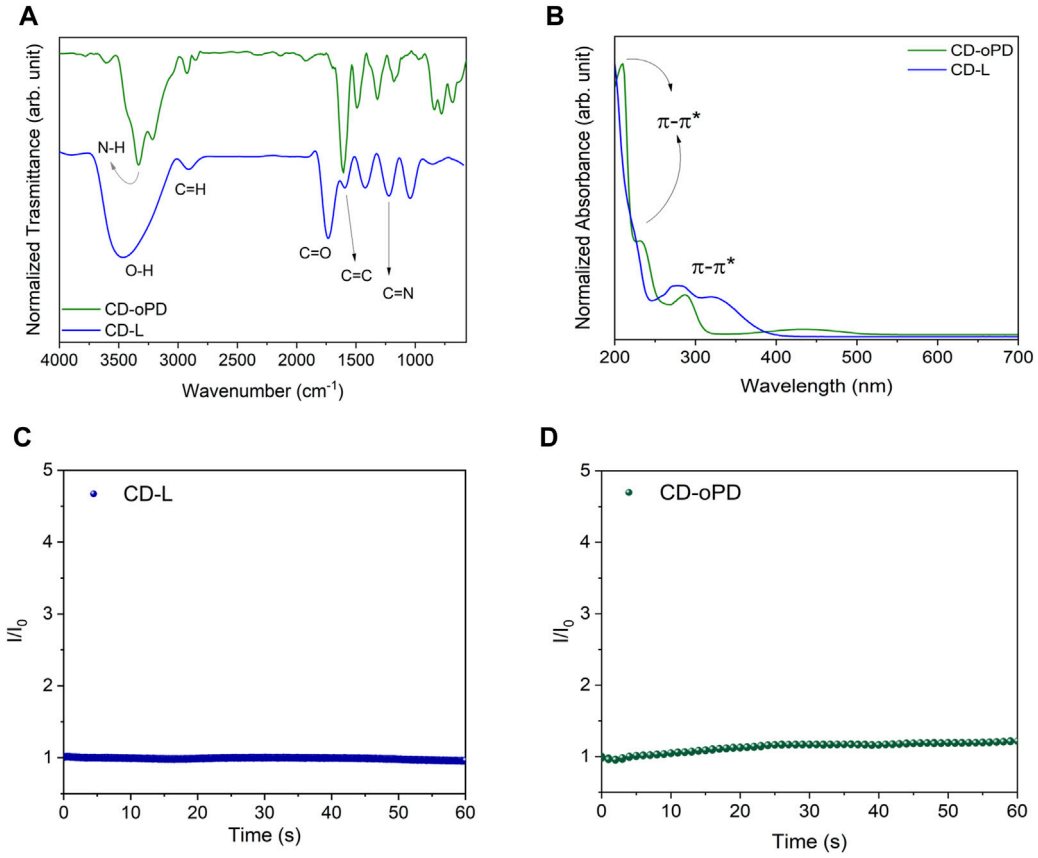

FIGURE 2
(A) FT-IR spectra for CD-L (blue line) and CD-oPD (green line), **(B)** UV-Vis absorption spectra for CD-L (blue line) and CD-oPD (green line), **(C)** Photostability under UV light (365 nm) for CD-L and **(D)** under UV light (350 nm) for CD-oPD.

real-time, *in situ* measurement of pH value and redox status in wounds.

2 Experimental

2.1 Chemicals

Tahiti lemons (Citrus latifolia) were obtained from local markets (SisGen access number: A4098F3). The chemicals o-phenylenediamine, boric acid, acetic acid, phosphoric acid, MTT [3-(4,5-dimethylthiazol-2-yl)-2,5-diphenyltetrazolium bromide], polyvinyl alcohol (PVA-average mol wt 89,000–98,000) and glycerol were acquired from Sigma-Aldrich (St. Louis, United States). Deionized water (18.2 MΩ cm) obtained from the Master System MS 2000 (Gehaka, Brazil) was used. Pig belly skin was purchased freshly from a local butcher.

2.2 Synthesis of lemon waste-derived carbon dots (CD-L)

The CD-L was synthesized according to the methodology reported by Silva et al., 2023. Briefly, the aqueous extract of Tahiti lemon was obtained using 60 g of the bagasse in 130 mL of deionized water, stirred for 60 min at 100°C. After heating, the mixture containing lemon bagasse was separated from the aqueous extract by filtration through a filtered through the fluted paper in a glass funnel. Fifty (50) mL of this resulting solution was heated using a domestic microwave (5 min, 720 W). Subsequently, 50 mL of deionized water was added to the solids resulting to obtain a suspension containing the CDs, since the solvent was completely evaporated during the reaction. The purification was carried by centrifugation of suspension at high speed (15,000 rpm), and filtration, using membranes of cellulose acetate (0.22 μm). The concentration of CD-L in the aqueous solution was ≈20 mg mL^{-1}. Finally, they were stored in a refrigerator at 4°C.

2.3 Synthesis of *o*-phenylenediamine-derived carbon dots (CD-oPD)

The CD-oPD was obtained by a simple hydrothermal reaction adapted from Davi et al. (2021). The reaction consisted of a mixture of 20 mg of *o*-phenylenediamine and 10 mL of deionized water in a stainless steel reactor, which was heated for 4 h at 200°C. The purification and storage of the

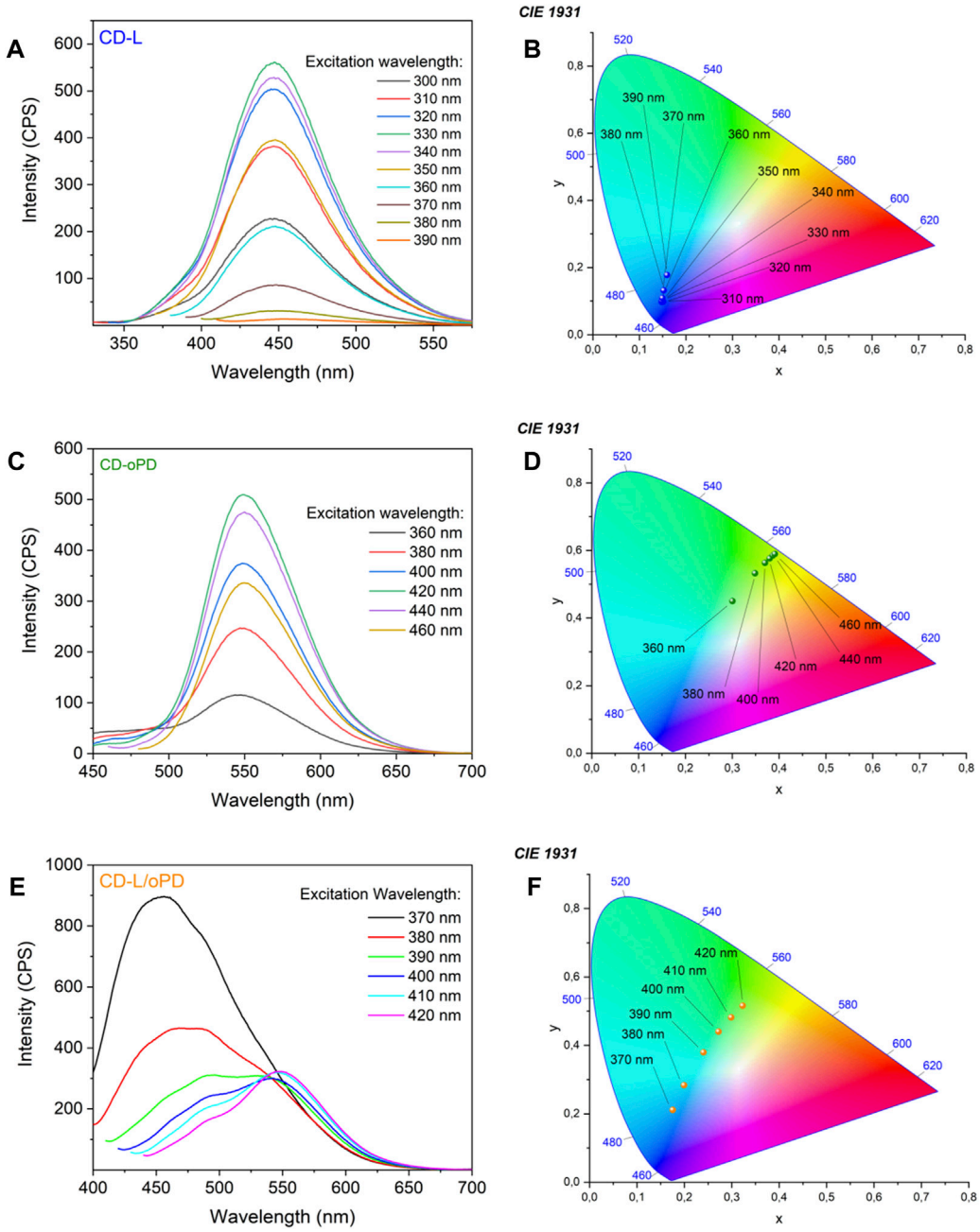

FIGURE 3
Photoluminescence spectra for **(A)** CD-L, **(B)** CD-oPD and **(C)** CD-L/oPD and CIE chromaticity diagram for **(D)** CD-L, **(E)** CD-oPD, and **(F)** CD-L/oPD.

CD-oPD was carried out according to the established protocol for CD-L.

2.4 Film of CD-L-F, CD-oPD -F and CD-L/oPD-F

The synthesis of the film CD-L/oPD-F was based on reported data (Elias et al., 2023). Briefly, 150 mg of PVA dissolved in 5 mL of deionized water under stirring at 80°C for 5 min. After cooling, 250, 125, and 60 µL of CD-L, CD-oPD, and glycerol were added to the solution, respectively. The mixture was stirred, deposited onto a plastic Petri dish (35 mm x 10 mm), and placed in an oven at 50°C for 48 h. The same procedure was used to synthesize film CD-L/CD-oPD-F, adding 250 µL of CD-L and 125 µL of CD-oPD.

2.5 *Ex-vivo* pH ratiometric sensor model

The pH ratiometric sensor assay using the CD-L/oPD-F film was carried out on pig belly skin samples *ex vivo*. Pieces of pig skin were cut uniformly in a 2 cm × 1.5 cm size and sprayed with different pH solutions ranging from 5 to 9 for 15 min according to previous studies (Tamayol et al., 2016). The CD-L-F or CD-oPD-F film was cut

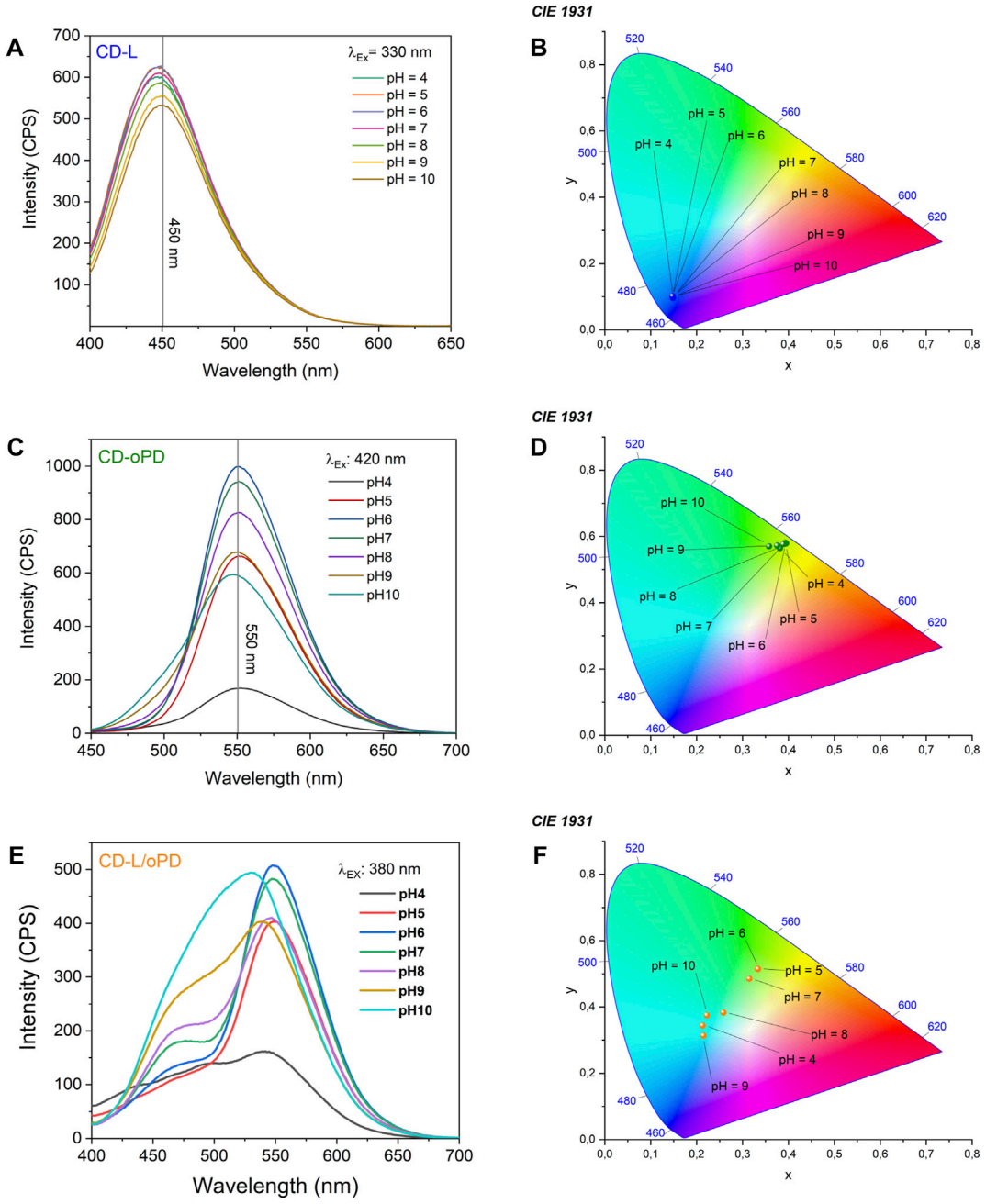

FIGURE 4
Photoluminescence spectra under different pH values for **(A)** CD-L, **(B)** CD-oPD and **(C)** CD-L/oPD and CIE chromaticity diagram for **(D)** CD-L, **(E)** CD-oPD and **(F)** CD-L/oPD.

in 1 cm × 1 cm and supported on the skin. After 30 min, the emission colors of the films were visualized through an ultraviolet lamp (360 nm).

2.6 Swelling test of the CD-L-F, CDs-oPD -F and CD-L/oPD-F films

The swelling assay was performed to evaluate the absorption and solubility of CD-L-F, CD-oPD-F and CD-L/oPD-F films in Britton-Robinson buffer solution at different pH. The films were cut into squares of 1.0 cm × 0.5 cm and immersed at intervals of time up to 90 min in a buffer solution at pH 5, 7 and 9 (≈37°C). Afterward, the films were removed from the solution and the excess buffer solution on the surface of the films was removed by blotting the surface with tissue paper (this procedure was carried out in triplicate). The swelling degree (%SW) was calculated according to Eq. 1, where M_t represents the mass of the film at intervals of time and M_0 represents the mass of the dry film at the initial time.

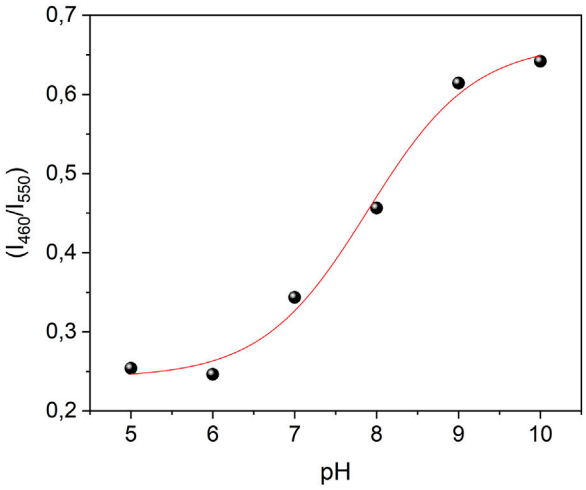

FIGURE 5
Sigmoidal fitting of the ratiometric fluorescent (I_{460}/I_{550}) CD-L/oPD in different pH.

$$\%SW = \frac{M_t\text{-}M_0}{M_0} \text{x } 100 \quad (1)$$

2.7 Characterization of materials

For Transmission Electron Microscopy (TEM) images, a JEM-2100 (JEOL, Japan) with a 200-kV accelerating voltage was used. The CDs for TEM measurements were prepared by diluting them 10-fold with ultrapure water, followed by dispersion in an ultrasonic bath, for 5 min and the resulting materials were deposited on 400-mesh carbon-coated Cu grids. To process our TEM microscopy images, we used ImageJ software for particle characterization. One hundred (100) particles were counted, and, based on this count, the average particle size for each CD synthesized was calculated. Fourier transform infrared spectroscopy (FTIR) spectra analysis of the CDs was carried out using Nicolet iS05 FTIR Spectrometer (Thermo Fisher Scientific, United States) and potassium bromide (KBr) pelleting method. To obtain the KBr pellets of the CDs, approximately 50 µL of the concentrated solution of CD-L and CD-oPD was dropped onto 20 mg of KBr. The sample was dried in an oven at 100°C for 24 h. The spectral range used for analysis was 4,000 to 400 cm^{-1}. The ultraviolet-visible (UV-Vis) absorption spectra of the CDs were acquired via Shimadzu UV/Vis/NIR Spectrometer UV-3600. The UV-Vis measurements of the films were carried on the aforementioned equipment using the solid-state system, in which the films were previously cut into a rectangular shape of 2 cm × 1.25 cm. Fluorescence spectroscopy analysis of the CDs in solution was carried out using a Shimadzu RF-5301PC Fluorescence Spectrophotometer. Solid-state measurements of the films were recorded using the Horiba-Jobin Yvon Fluorolog-3 spectrofluorometer. The emission modulation of CD-L and CD-*o*PD to obtain the ratiometric system was performed based on the photoluminescence spectrum of the sample and analyzed while varying the quantity of CDs. Thus, the obtained CD-L and CD-oPD were mixed in a ratio of 2:1 to produce the ratiometric system CD-L/oPD. The FL of the CDs (CD-L, CD-oPD and CD-L/oPD) as a function of pH was then measured using a Shimadzu RF-5301PC spectrofluorimeter. For this purpose, 50 and 25 µL of CD-L and CD-oPD, respectively, were added to 2 mL of pH solution (4–10). CD-L/oPD was measured by mixing 50 and 100 µL of CD-L and CD-oPD, respectively, in 2 mL of pH solution (4–10). The pH 4 to 10 solutions were prepared using Britton Robinson buffer (BR buffer) (0.1 mol/L), which was prepared using acetic, boric and phosphoric acids, all at a concentration of 0.4 mol/L. The acids were mixed and analyzed in a pHmeter to obtain the required pH value. Solutions of hydrochloric acid and sodium hydroxide (1 mol/L) were used to calibrate the solutions from pH 4 to 10. The photostability of the CDs was evaluated using photoluminescence spectroscopy. 50 and 25 µL of CD-L and CD-oPD, respectively, were added separately to 2 mL of water in a quartz cuvette. The fluorescence intensity (FI) of CD-L and CD-oPD was recorded under UV lamp excitation at 365 and 350 nm with emission monitored at 450 and 550 nm, respectively. Analyses were carried out for 60 min continuously, with the sample partially irradiated. The CIE 1931 chromaticity color coordinates diagram were obtained using the emission spectra of the all materials from the software Origin Pro.

2.8 Viable cells assay

To determine the biocompatibility of CD-oPD, MTT assay was used as previously reported (Mosmann, 1983; Silva et al., 2023). Human skin fibroblast lineage (HFF-1) cells were grown in 96-well plates, treated with different concentrations (0–1,000 µg mL^{-1}) and incubated for 24 h at 37°C, in a CO_2 incubator. After that, the optical density (OD) of the cells was measured at 540 nm using a spectrophotometer leading to viability (%), according to Eq. 2:

$$\text{Viability (\%)} = (\text{OD of treated cells}/\text{OD of untreated cells}) \times 100 \quad (2)$$

For statistical analysis of viable cell results, the ANOVA one-way test was used and data were compared using Tukey's method. The statistically significant difference accepted was $p < 0.05$.

2.9 Hypochlorous acid (HOCl) scavenging activity

The HOCl scavenging activity was performed according to Lucas et al. (2021). An HOCl solution was prepared at the time of analysis by adjusting the pH value of a 1% (v/v) NaOCl solution to 6.2 with H_2SO_4 addition. The reaction system consisted of the addition of phosphate buffer (100 mM, pH 7.4), CD-L or CD-oPD (3–100 µg mL^{-1}) solution, dihydrorodamine solution (DHR, 5 µM), and HOCl (5 µM). Fluorescence measurements were performed in a microplate reader (Infinite® 200 PRO, TECAN, Männedorf, Switzerland), at 310 K, at wavelengths of 505 ± 10 nm and 530 ± 10 nm, for excitation and emission,

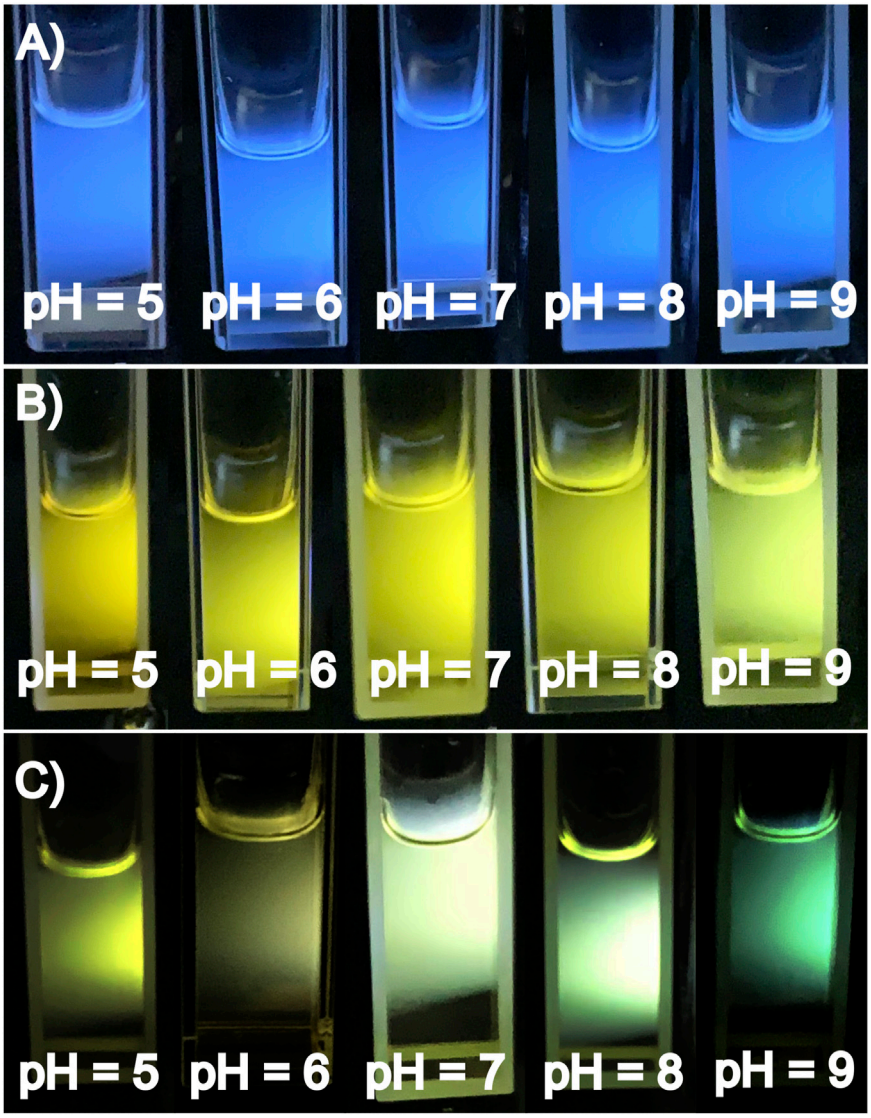

FIGURE 6
(A) Photographs of CD-L, **(B)** CD-oPD and **(C)** CD-L/oPD under different pH variations (pH = 5–9) under 360 nm UV lamp.

respectively. The results were expressed as the half-maximal inhibitory concentration (IC_{50}) in μg mL^{-1}.

2.10 Radical superoxide anion scavenging activity

The radical superoxide anion scavenging activity was determined according to Lucas et al. (2021). In a 96-well plate, the following solutions were added to the indicated final concentrations: CD-L (3–800 μg mL^{-1}) or CD-oPD (3–1,000 μg mL^{-1}), NADH (166 μM), NBT (43.3 μM) and PMS (2.7 μM). Potassium phosphate buffer (19 mM, pH 7.4) was used to dissolve CD-L, NADH, NBT, and PMS. Quercetin was used as a standard for comparison purposes. The experiment was conducted at 310 K in a microplate reader, and the absorbance was measured at 560 nm. The results were expressed as IC_{50} in μg mL^{-1}.

2.11 DPPH• scavenging assay

The evaluation of the reducing capacity of DPPH$^{\bullet}$ was conducted as previously described (Xavier et al., 2017). Briefly, aliquots of CD-L or CD-oPD (5–100 μg mL^{-1}) were added to a DPPH$^{\bullet}$ solution (40 μg mL^{-1} in methanol). Measurements were taken at 516 nm after 30 min of incubation in the dark, using a UV-Vis spectrophotometer (Agilent Technologies, Santa Clara, CA, United States). The results were expressed as IC_{50} in μg mL^{-1}.

3 Results and discussion

CD-L and CD-oPD were obtained by a simple and rapid method via microwave and hydrothermal procedures, respectively (Davi et al., 2021; Silva et al., 2023). TEM was used to provide information about the CDs morphology and size. In this regard, the TEM images

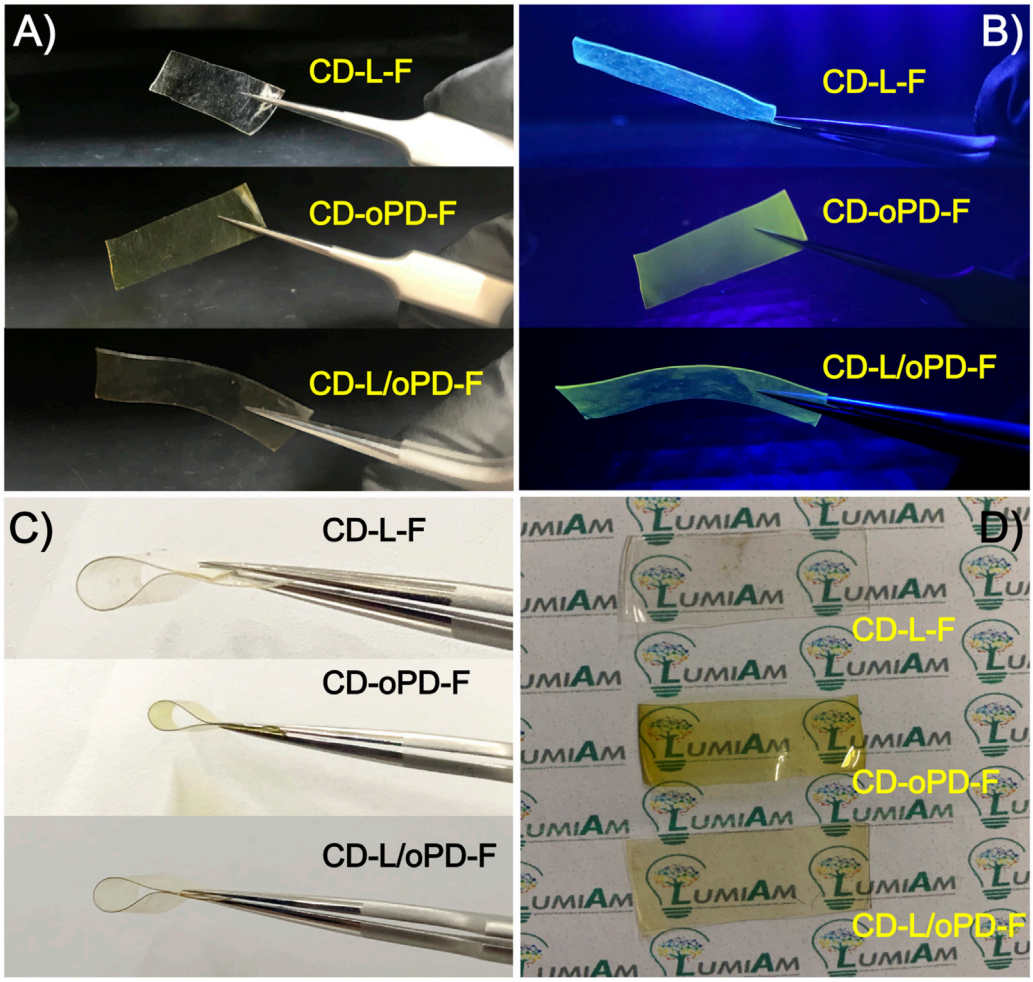

FIGURE 7
(A,B) Image before and after exposure to ultraviolet light, **(C)** flexibility tests and **(D)** transparency for CD-L-F, CD-oPD-F and CD-L/oPD-F.

showed that both CD-L and CD-oPD exhibited spherical graphitic morphology with uniform size dispersion, and average values of 2.54 ± 0.44 nm and 2.64 ± 0.60 nm, respectively (Figures 1A–C). In the magnified image displayed in Figures 1B–D, the interplanar distances typical of the graphitic structure can be observed for both carbon dots, which exhibited values of 0.21 and 0.24 nm corresponding to the diffraction plane (100) for CD-L and CD-oPD, respectively (Nascimento et al., 2023).

Fourier transform infrared spectroscopy (FTIR) was used to identify, in the CDs, the absorption peaks of the main functional groups (Figure 2A). The FTIR spectra revealed a broad and intense band attributed to the vibration of O-H stretching at around 3,445 and 3,330 cm^{-1} for CD-L and CD-oPD, respectively (He et al., 2022; Wang et al., 2022; Venugopalan and Vidya, 2023). In addition, for the CD-oPD this region includes the N-H axial deformation vibration at 3,220 cm^{-1} (Yang et al., 2019). For both CDs, it is also possible to observe C-H (sp^3) vibrations between 2,970 and 2,700 cm^{-1} (Döring et al., 2022; Jing et al., 2023). CD-L shows broad bands centered at 1722, 1,398 and 1,205 cm^{-1} suggestive of the presence C=O, C=C and C-N, associated with oxygenated groups, polyaromatic in its graphitic core and surface-functionalizing nitrogen groups, respectively (Ding et al., 2017; Ding et al., 2019). For CD-oPD, FTIR reveals peaks characteristic of aromatic C-N and N-H angular deformation associated with aromatic chain bonds observed at 1,330 and 780 cm^{-1}, respectively (Yang et al., 2019).

UV-Vis absorption spectroscopy revealed the π-π* electronic transitions of C=C bonds in the CD-L and CD-oPD graphitic nucleus, with bands centered at 225, 210 and 230 nm, respectively (Figure 2B) (Tadesse et al., 2018; Hui, 2023). In contrast, the n-π* transitions from C=O and C-N bonds can be observed in 278 e 320 nm for CD-L, and 290 e 430 nm for CD-oPD, respectively (Lu et al., 2021; Gedda et al., 2023). The photostability of the CDs was assessed using photoluminescence spectroscopy, with the fluorescence intensity (FI) recorded under UV lamp excitation for 60 min continuously (Figures 2C, D). The FI results for CD-L and CD-oPD remained practically unchanged during the analyzed period, with variations in the fluorescence signal of less than 10% (El-Shafey and Asma, 2021; Javed and O'Carroll, 2021).

Photoluminescence spectroscopy (PL) was used to investigate the luminescent properties of the CDs. CD-L and CD-oPD exhibit excitation-independent emission and the fluorescence spectrum.

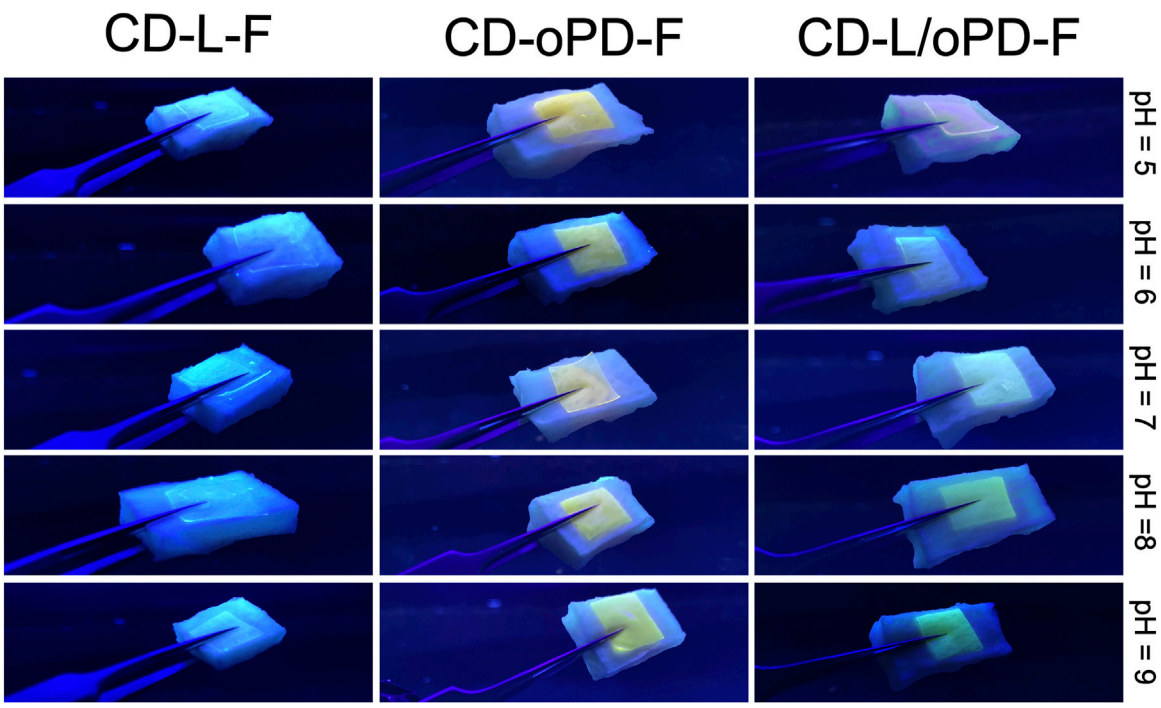

FIGURE 8
CD-L-F, CD-oPD-F, CD-L/oPD-F films supported on pieces of pig skin with different pH values.

CD-L revealed an emission band maximum centered in the blue region, at 450 nm (λ_{exc} = 330 nm) (Figure 3A). CD-oPD exhibits emission in the yellowish-green region with a maximum centered at 550 nm (λ_{exc} = 420 nm) (Figure 3C). The CDs behaviors clearly followed the chromaticity diagram, formulated by the Commission Internationale de L'Eclairage (CIE) (Figure 3B–D). Researchers have associated the independent emission of excitation wavelength (λ_{exc}) to some features of CDs, such as their uniform sizes, the presence of molecular states and/or similar groups on the surface with passivated defects (Li et al., 2014; Singh et al., 2022; Wei et al., 2023).

Under optimized conditions, solutions of CD-L and CD-oPD were mixed and it was possible to observe a fluorescence dual emission with bands centered on 450 nm and 550 nm (Figure 3E), which are consistent with the individual spectra of CD-L and CD-oPD, respectively. CD-L/oPD color coordinate points obtained from the CIE chromaticity diagram showed a clear distinction between blue and yellowish-green when the excitation wavelength increased from 370 to 420 nm (Figure 3F).

The analytical CDs response to pH variation was investigated using PL. CD-L results demonstrate that the fluorescence intensity rises with the pH increase from 4 to 5. On the other hand, fluorescence intensity decreases from pH 6 to 10 (Figure 4A). This behavior can be explained by the protonation/deprotonation mechanism, in which, after pH 7, the oxygenated groups present on the surface of CD-L are deprotonated, causing a decrease in their fluorescence intensity (Ehtesabi et al., 2020; Liu et al., 2021). In addition, the emission region did not change, remaining blue, as shown in the images of the CIE chromaticity diagram (Figure 4B).

The emission of CD-oPD was also monitored as a function of pH variation. Figure 4C shows that the fluorescence intensity gradually increased up to pH 6, after which it gradually decreased up to pH 10. This profile is similar to that of CD-L and can be explained by the same protonation/deprotonation mechanism. It can also be seen from the CIE chromaticity diagram that the emission region of CD-oPD remained in the green region (Figure 4D). Therefore, from these results, it was shown that individual CDs are unable to monitor wound healing efficiently, due to the difficult detection of color and/or fluorescence variations (Song et al., 2017; Lei et al., 2020; Xu et al., 2020; Li et al., 2021).

In this sense, a ratiometric system CD-L/oPD was developed using an optimized mixture of CD-L and CD-oPD, where the modulated resulting solutions show an excellent ratiometric colorimetric response as a function of pH (Figure 4E). From the CIE chromaticity diagram it was possible observing that the emission of CD-L/oPD aqueous solution, even with naked eyes, varied from yellowish-green to green (Figure 4F). The ratiometric system showed a high sensitivity for detecting pH in the range of 5–10. This interval, as mentioned previously, is suitable for monitoring the wound healing process. The pH response as a function of the intensity ratio (I_{460}/I_{550}) fits well to a sigmoidal curve (Figure 5), as shown in Equation 3, with an r^2 = 0.992.

$$y = 0.24 + \frac{0.66 - 0.24}{1 + 10^{0.67x\,(log\,(0-x))}} \quad (3)$$

On the other hand, CD-L and CD-oPD show a linear function in the pH range from 6 to 10. The linear fitting equation was y = 763.0–22.8x with r^2 = 0.991 and y =1,666.8–107.5x with r^2 = 0.983 for CD-L and CD-oPD, respectively (Supplementary Figures S1, S2).

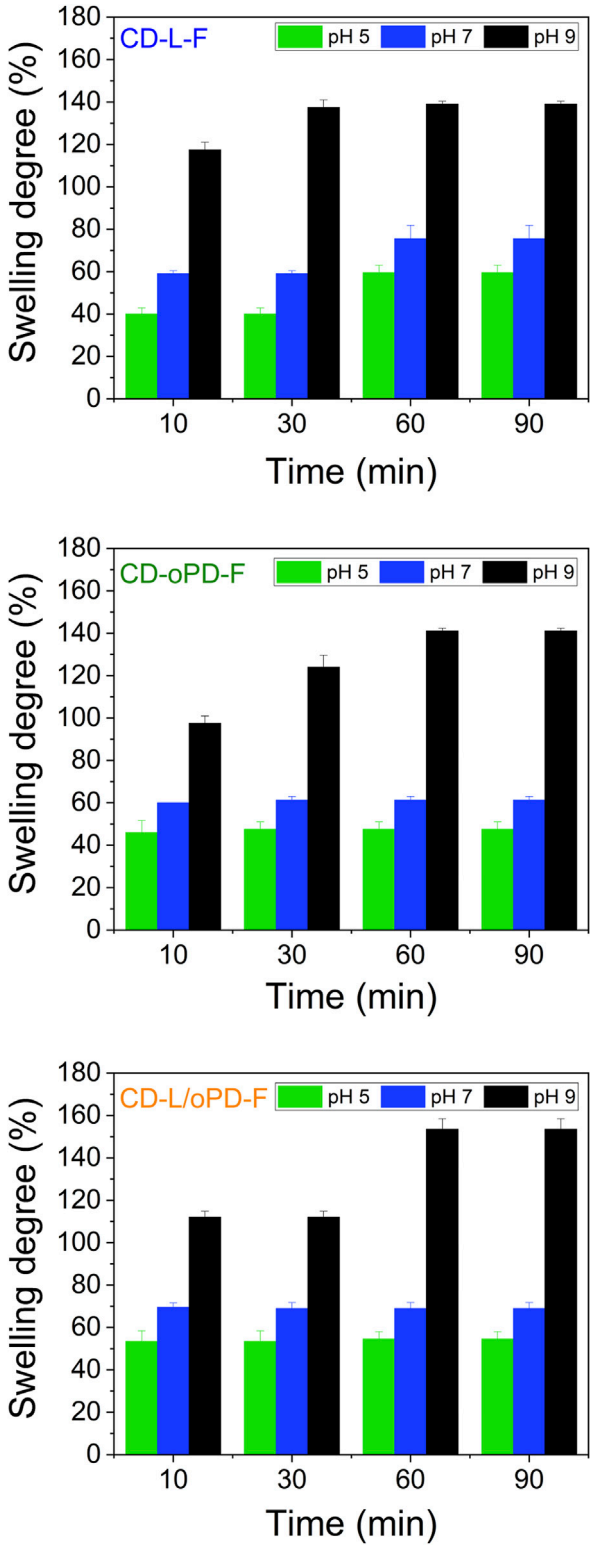

FIGURE 9
Swelling kinetics for CD-L-F, CD-oPD-F and CD-L/oPD-L in different pH values.

The data presented in Figures 4A–C, related to the influence of pH for CD-L, CD-oPD and CD-L/oPD, together with the photographs of the solutions (Figures 6A–C), indicate their corresponding trends, as expected. Hence, the CD-L results demonstrate a blue emission with no perceptible change to the naked eye. Similarly, the CD-oPD results reveal a consistent yellow emission, except at pH 9, where a pale yellowish-green color was observed. In contrast, the CD-L/oPD ratiometric system exhibits a gradient of emission color changes from yellowish-green to green with the pH varying from 5 to 9.

Both the individual nanocompounds, the CD-L and CD-oPD, and the combined one, the CD-L/oPD, were incorporated into PVA to obtain fluorescent polymeric films able to detect pH variation. Under natural light, the films obtained were colorless for CD-L-F and yellowish for CD-oPD-F and CD-L/oPD-F (Figure 7A). On the other hand, under UV light, the characteristic blue emission of CD-L was observed for CD-L-F, and yellow and yellowish-green for CD-oPD and CD-L/oPD films, respectively (Figure 7B). In addition, the fluorescent films exhibited flexibility and transparency, which can be seen in Figures 7C, D). The maximum emission wavelength of CD-L-F and CD-oPD-F shifted towards blue compared to CDs in solution. The maximum emission intensity of the CD-L-F film is at 425 nm (λ_{Exc} = 320 nm) (Supplementary Figure S3A), while CD-L in solution exhibits the maximum emission at 450 nm (λexc = 330 nm) (Figure 3A). Similarly, the maximum emission of the CD-oPD-F film occurred at 525 nm (λ_{Exc} = 410 nm) (Supplementary Figure S3B), compared to CD-oPD in solution with a maximum emission intensity of 550 nm (λ_{Exc} = 420 nm) (Figure 3B). Furthermore, when comparing CD-L/oPD solution and CD-L/oPD-F film, it can be observed that although they exhibit a similar profile in terms of the emission spectrum in the 400–650 nm range, the relative intensities of the emission bands at 450 and 550 nm have changed. In this context, it is suggested that these changes in the emission maximum or intensity ratio of the CDs in solution and in the PVA films occur due to the formation of hydrogen bonds between the PVA and the surface functional groups of the CDs when the nanoparticles are stabilized in the polymer (Bandi et al., 2018; Taspika et al., 2019). Despite the reported changes, the emission color of the films demonstrated similar behavior to those presented in solution.

For the simulation test, pork skin was exposed to solutions with different pH values in the range of 5–9, Figure 8. The prepared films were placed on the pork skin previously sprayed with different pH solutions and after 30 min they were exposed to UV radiation and a behavior similar to that previously found in the solution was clearly observed. As the pH increased from 5 to 9, a color change was observed to CD-L/oPD-F from greenish-yellow to green, respectively.

The values of the swelling degree (%SW) at different pH values of the films produced are shown in Figure 9. Overall, the degree of swelling of the films increased with pH and time reached equilibrium in 60 min. The minimum and maximum %SW values of the films at pH 5, 7 and 9 were 47.5–59.5, 59.0–75.5 and 97.5–153.5, respectively. These values were suitable to maintain the shape and uniform edges of the films, after the swelling tests (Supplementary Figures S4–S6). The swelling response as a function of pH can be attributed to ionizable functional groups of the PVA (OH) and CDs (OH and COOH), which promote an electrostatic repulsion and

TABLE 1 DPPH$^{\bullet}$, $O_2^{\bullet-}$ and HOCl scavenging potential (IC_{50}, mean ± SD) of CD-L and CD-oPD.

Sample	$O_2^{\bullet-}$ IC_{50} (μg mL^{-1})	HOCl IC_{50} (μg mL^{-1})	DPPH$^{\bullet}$ IC_{50} (μg mL^{-1})
CD-L	272.8 ± 3.3	25.1 ± 0.5	56.7 ± 0.2
CD-oPD	[a]	63.4 ± 3.8	39.5 ± 0.4
Quercetin	26.6 ± 3.7	5.6 ± 1.0	2.8 ± 0.2

[a]Inactive until the concentration of 1,000 μg mL−1.

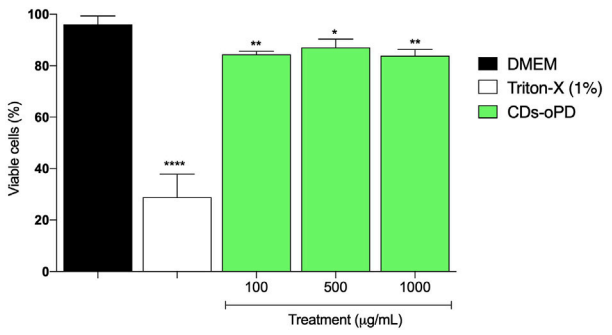

FIGURE 10
MTT assay results of the treatment of the HFF-1 cells with CD-oPD (100–1,000 μg mL^{-1}). Bars represent the mean ± standard error of the mean (SEM) of triplicates performed in the assay. Data are expressed as % viable cells compared to the control group (DMEM). Results were analyzed using GraphPad Prism software using ANOVA followed by Tukey's post-test, *p <0.05 and **p <0.01 (DMEM vs. treatment).

increase interactions with water in the function of the increase of pH (Naeem et al., 2017; Kalantari et al., 2020; Sabzi et al., 2020; Akhlaq et al., 2021; Suhail et al., 2021). As a result, an expansion of the film is observed creates a greater surface area available for the diffusion of water molecules, which leads to a significant increase in the degree of absorption of the medium. (Zafar et al., 2023).

The antioxidant capacity of CDs has been extensively examined and is attributed to the functional groups present on their surface that can stabilize reactive species through mechanisms of electron transfer or hydrogen atom transfer. The DPPH$^{\bullet}$ assay is the most commonly employed method because it is fast, easy, and economically viable; however, it is not a physiologically relevant reactive species. In this study, in addition to evaluating the antioxidant capacity of CD-oPD and CD-L against DPPH$^{\bullet}$, we also examined their potential to eliminate two biologically relevant reactive species: $O_2^{\bullet-}$ and HOCl (Table 1).

CD-L exhibited higher antioxidant capacity against physiological reactive species such as $O_2^{\bullet-}$ and HOCl. CD-oPD showed no elimination capacity against $O_2^{\bullet-}$, however, it demonstrated a greater potential for capturing the DPPH radical, with a lower IC_{50}. CDs derived from Beta vulgaris (beet juice) exhibited an IC_{50} of 231.7 μg mL^{-1} (Smrithi et al., 2022), value higher than those obtained in this study, indicating greater potential for reducing DPPH$^{\bullet}$ by CD-oPD and CD-L (Table 1). CDs derived from cloves exhibited an IC_{50} value (57 μg mL^{-1}) (Pandey et al., 2022) similar to that obtained for CD-L and higher than that obtained for CD-oPD (Table 1). Clove-derived CDs were also assessed against $O_2^{\bullet-}$ and showed an IC_{50} of 53 μg mL^{-1} (Pandey et al., 2022), indicating greater activity against this reactive species, compared to CD-L.

The samples were evaluated for their biocompatibility (absence of cytotoxicity) by the MTT method. As shown in Figure 10, cells exposed to CD-oPD showed viability greater than 80% at all concentrations tested, similar to cells treated with CD-L (Silva et al., 2023), corroborating the relatively negligible cytotoxicity of the CDs in non-transformed human fibroblasts HFF-1 cells. Cells treated with triton-X (1%) were used as a control for reduced cell viability (28% of viable cells) (Arechabala et al., 1999; Goiato et al., 2023). In comparison with other CDs and nanomaterials reported in the literature, the cell viability of CD-oPD in human fibroblasts (HFF-1 cells) exhibited more prominent cell viability (Supplementary Table S1).

Although carbon dots have been explored as fluorescent pH sensors, there are still few studies on their use for monitoring pH in wounds, since this parameter changes during the healing process. In addition, systematic studies aimed at combining different properties to offer both monitoring and treatment of wound healing are still rare (Omidi et al., 2017; Yang et al., 2019; Liu et al., 2021; Liu et al., 2021). In this sense, this work seeks to combine the use of CDs in the form of films to act as an antioxidant agent, protective barrier and colorimetric pH sensor in wounds with a view to their use as bioactive dressings.

4 Conclusion

Carbon dots (CD) derived from lemon peel bagasse (L) and *o*-phenylenediamine (*o*-PD) were prepared via simple microwave and hydrothermal methods, respectively. The blue fluorescence of CD-L and the yellow-green of CD-oDP were successfully explored in the preparation of a highly efficient dual-emissive system CD-L/oPD for pH detection. Polymeric films based on PVA and a mixture of CD-L and CD-oPD were prepared and when applied on pig skin, they displayed a significant change in the wavelength of the emission line from greenish-yellow to green with the increase of the pH values from 5 to 9. In addition, the CDs exhibited low cytotoxicity in human fibroblasts HFF-1 cells and relevant antioxidant capacity. Finally, the fluorescent film based on a CD ratiometric system may have potential for monitoring the *in-situ* pH of wounds.

Data availability statement

The original contributions presented in the study are included in the article/Supplementary Material, further inquiries can be directed to the corresponding author.

Author contributions

LS: Conceptualization, Investigation, Methodology, Visualization, Writing–original draft, Writing–review and editing. AA: Investigation, Methodology, Visualization, Writing–review and editing. JA: Investigation, Methodology, Visualization, Writing–review and editing. LD: Investigation, Methodology, Writing–review and editing, Visualization. MS: Investigation, Methodology, Visualization, Writing–review and editing. DL: Investigation, Visualization, Writing–review and editing, Resources. RV: Conceptualization, Investigation, Visualization, Writing–review and editing. JF: Investigation, Methodology, Resources, Visualization, Writing–review and editing. MG: Investigation, Resources, Visualization, Writing–review and editing. JX: Investigation, Methodology, Resources, Visualization, Writing–review and editing. CB: Conceptualization, Investigation, Project administration, Resources, Supervision, Writing–original draft, Writing–review and editing, Visualization.

Funding

The author(s) declare that financial support was received for the research, authorship, and/or publication of this article. The authors gratefully acknowledge the financial support of the Brazilian research funding agencies CAPES (Coordination for the Improvement of Higher Education Personnel) for fellowships (88887.636268/2021-00) and FAPEAL (N°: 60030.0000002294/2022) for financial support.

Acknowledgments

The authors thank the Universidade Federal de Alagoas (UFAL). RV expressed their appreciation for fellowships granted by FAPEAL/CNPq (Grant No. DCR2022051000008). The authors would like to thank Tatiane Oliveira dos Santos and Laboratório Multiusuário de Microscopia de Alta Resolução (LabMic) of the University of Goiás, Brazil, for HRTEM measurements. Optics and Nanoscopy Group (GON) for providing the infrastructure to perform the characterizations optical of CDs.

Conflict of interest

The authors declare that the research was conducted in the absence of any commercial or financial relationships that could be construed as a potential conflict of interest.

Publisher's note

All claims expressed in this article are solely those of the authors and do not necessarily represent those of their affiliated organizations, or those of the publisher, the editors and the reviewers. Any product that may be evaluated in this article, or claim that may be made by its manufacturer, is not guaranteed or endorsed by the publisher.

Supplementary material

The Supplementary Material for this article can be found online at: https://www.frontiersin.org/articles/10.3389/frcrb.2023.1300811/full#supplementary-material

References

Akhlaq, M., Azad, A. K., Ullah, I., Nawaz, A., Safdar, M., Bhattacharya, T., et al. (2021). Methotrexate-Loaded gelatin and polyvinyl alcohol (gel/PVA) hydrogel as a pH-sensitive matrix. *polymers* 13 (14), 2300. doi:10.3390/polym13142300

Arechabala, B., Coiffard, C., Rivalland, P., Coiffard, L. J. M., and Roeck-Holtzhauer, Y. D. (1999). Comparison of cytotoxicity of various surfactants tested on normal human fibroblast cultures using the neutral red test, MTT assay and LDH release. *J. Appl. Toxicol.* 19 (3), 163–165. doi:10.1002/(SICI)1099-1263(199905/06)19:3<163::AID-JAT561>3.0.CO;2-H

Bandi, R., Devulapalli, N. P., Dadigala, R., Gangapuram, B. R., and Guttena, V. (2018). Facile conversion of toxic cigarette butts to N,S-codoped carbon dots and their application in fluorescent film, security ink, bioimaging, sensing and logic gate operation. *ACS Omega* 3 (10), 13454–13466. doi:10.1021/acsomega.8b01743

Bankoti, K., Rameshbabu, A. P., Datta, S., Das, B., Mitra, A., and Dhara, S. (2017). Onion derived carbon nanodots for live cell imaging and accelerated skin wound healing. *J. Mater. Chem. B* 5 (32), 6579–6592. doi:10.1039/c7tb00869d

Cui, F., Sun, J., Ji, J., Yang, X., Wei, K., Xu, H., et al. (2021). Carbon dots-releasing hydrogels with antibacterial activity, high biocompatibility, and fluorescence performance as candidate materials for wound healing. *J. Hazard. Mater.* 406, 124330. doi:10.1016/j.jhazmat.2020.124330

da Silva, K. R. M., Calado, C. M. S., dos Santos, T. V., Sales, T. O., Viana, R. S., Silva, U. R., et al. (2022). Plate-like CDots/EuBDC nanocomposite for ratiometric luminescence thermometry. *J. Mater. Chem. C* 10 (32), 11614–11624. doi:10.1039/d2tc01587k

da Silva, L. E., Calado, O. L. L., de Oliveira Silva, S. F., da Silva, K. R. M., Henrique Almeida, J., de Oliveira Silva, M., et al. (2023). Lemon-derived carbon dots as antioxidant and light emitter in fluorescent films applied to nanothermometry. *J. Colloid Interface Sci.* 651, 678–685. doi:10.1016/j.jcis.2023.07.124

Davi, L. B. D. O., Lima, DJDP, and Barbosa, CDDES (2021a). SÍNTESE DE CARBON DOTS A PARTIR DE DERIVADOS DE ANILINA A FIM DE AVALIAR O EFEITO DOS SUBSTITUINTES NAS PROPRIEDADES FOTOFÍSICAS E ESTRUTURAIS/SYNTHESIS OF CARBON DOTS FROM ANILINE DERIVATIVES IN ORDER TO EVALUATE THE EFFECT OF SUBSTITUENTS ON PHOTOPHYSICAL AND STRUCTURAL PROPERTIES. *Braz. J. Dev.* 7 (1), 2732–2743. doi:10.34117/bjdv7n1-186

Davi, L. B. O., Lima, D., and Barbosa, C. (2021b). Synthesis and modulation of multicolor fluorescent carbon dots from p-phenylenediamine and dansyl derivative for white light emitting diodes. *Opt. Mater.* 121, 111502. doi:10.1016/j.optmat.2021.111502

Ding, H., Ji, Y., Wei, J. S., Gao, Q. Y., Zhou, Z. Y., and Xiong, H. M. (2017). Facile synthesis of red-emitting carbon dots from pulp-free lemon juice for bioimaging. *J. Mater. Chem. B* 5 (26), 5272–5277. doi:10.1039/c7tb01130j

Ding, H., Li, X. H., Chen, X. B., Wei, J. S., Li, X. B., and Xiong, H. M. (2020). Surface states of carbon dots and their influences on luminescence. *J. Appl. Phys.* 127 (23), 231101. doi:10.1063/1.5143819

Ding, H., Zhou, X., Qin, B., Zhou, Z., and Zhao, Y. (2019). Highly fluorescent near-infrared emitting carbon dots derived from lemon juice and its bioimaging application. *J. Luminescence* 211, 298–304. doi:10.1016/j.jlumin.2019.03.064

Dong, C., Ma, X., Huang, Y., Zhang, Y., and Gao, X. (2022). Carbon dots nanozyme for anti-inflammatory therapy via scavenging intracellular reactive oxygen species. *Front. Bioeng. Biotechnol.* 10, 1–8. doi:10.3389/fbioe.2022.943399

Döring, A., Ushakova, E., and Rogach, A. L. (2022). Chiral carbon dots: synthesis, optical properties, and emerging applications. *Light Sci. Appl.* 11 (1), 75–23. doi:10.1038/s41377-022-00764-1

Ehtesabi, H., Hallaji, Z., Najafi Nobar, S., and Bagheri, Z. (2020). Carbon dots with pH-responsive fluorescence: a review on synthesis and cell biological applications. *Microchim. Acta* 187 (2), 150. doi:10.1007/s00604-019-4091-4

Elias, L., Orlando Lucas de L. Calado, and Cintya D. A. do E. S. Barbosa, (2023). Study of the photophysical properties of carbon dots derived from banana peels from different cities used to produce ink and film fluorescence. *J. Bioeng. Technol. health* 5, 250–256. doi:10.34178/jbth.v5i4.247

El-Shafey, A. M., and Asma, M. (2021). Carbon dots: discovery, structure, fluorescent properties, and applications. *Green Process. Synthesis* 10, 134–156. doi:10.1515/gps-2021-0006

Farshidfar, N., Fooladi, S., Nematollahi, M. H., and Iravani, S. (2023). Carbon dots with tissue engineering and regenerative medicine applications. *RSC Adv.* 13 (21), 14517–14529. doi:10.1039/d3ra02336b

Gedda, G., Sankaranarayanan, S. A., Putta, C. L., Gudimella, K. K., Rengan, A. K., and Girma, W. M. (2023). Green synthesis of multi-functional carbon dots from medicinal plant leaves for antimicrobial, antioxidant, and bioimaging applications. *Sci. Rep.* 13 (1), 6371–6379. doi:10.1038/s41598-023-33652-8

Goiato, M., Marobo, A., Caxias, F., da Silva, E., Gonçalves, L., Oliveira, S., et al. (2023). Cytotoxicity of cleaning agents for ocular prostheses. *Polym. Med.* 53 (1), 37–46. doi:10.17219/pim/163118

He, C., Xu, P., Zhang, X., and Long, W. (2022). The synthetic strategies, photoluminescence mechanisms and promising applications of carbon dots: current state and future perspective. *Carbon* 186, 91–127. doi:10.1016/j.carbon.2021.10.002

Huangfu, S., Jin, G., Sun, Q., Li, L., Yu, P., Wang, R., et al. (2021). The use of crude carbon dots as novel antioxidants for natural rubber. *Polym. Degrad. Stab.* 186, 109506. doi:10.1016/j.polymdegradstab.2021.109506

Hui, S. (2023). Carbon dots (CDs): basics, recent potential biomedical applications, challenges, and future perspectives. *J. Nanoparticle Res.* 25, 68. doi:10.1007/s11051-023-05701-w

Javed, N., and O'Carroll, D. M. (2021). Carbon dots and stability of their optical properties. *Part. Part. Syst. Charact.* 38 (4), 1–12. doi:10.1002/ppsc.202000271

Jin, S. G. (2022). Production and application of biomaterials based on polyvinyl alcohol (PVA) as wound dressing. *Chem. Asian J.* 17 (21), 2022005955–e202200613. doi:10.1002/asia.202200595

Jing, H. H., Bardakci, F., Akgöl, S., Kusat, K., Adnan, M., Alam, M., et al. (2023). Green carbon dots: synthesis, characterization, properties and biomedical applications. *J. Funct. Biomaterials* 14 (1), 27–32. doi:10.3390/jfb14010027

Juan, C., Pérez de la Lastra, J. M., Plou, F. J., and Pérez-Lebeña, E. (2021). The chemistry of reactive oxygen species (ROS) revisited: outlining their role in biological macromolecules (DNA, lipids and proteins) and induced pathologies. *Int. J. Mol. Sci.* 22, 4642. doi:10.3390/ijms22094642

Kadam, S., Nadkarni, S., Lele, J., Sakhalkar, S., Mokashi, P., and Kaushik, K. S. (2019). Bioengineered platforms for chronic wound infection studies: how can we make them more human-relevant? *Front. Bioeng. Biotechnol.* 7, 418. doi:10.3389/fbioe.2019.00418

Kalantari, K., Mostafavi, E., Saleh, B., Soltantabar, P., and Webster, T. J. (2020). Chitosan/PVA hydrogels incorporated with green synthesized cerium oxide nanoparticles for wound healing applications. *Eur. Polym. J.* 134, 109853. doi:10.1016/j.eurpolymj.2020.109853

Kasouni, A. I., Chatzimitakos, T. G., Troganis, A. N., and Stalikas, C. D. (2021). Citric acid-based carbon dots: from revealing new insights into their biological properties to demonstrating their enhanced wound healing potential by *in vitro* and *in vivo* experiments. *Mater. Today Commun.* 26, 102019. doi:10.1016/j.mtcomm.2021.102019

Lei, X., Fu, Y., Wu, Y., Chen, L., and Liang, J. (2020). A ratiometric fluorescent probe for pH detection based on Ag 2 S quantum dots-carbon dots nanohybrids: ratiometric fluorescent pH probe. *R. Soc. Open Sci.* 7, 200482. doi:10.1098/rsos.200482

Li, S., Song, X., Hu, Z., and Feng, G. (2021). A carbon dots-based ratiometric fluorescence probe for monitoring intracellular pH and bioimaging. *J. Photochem. Photobiol. A Chem.* 409, 113129. doi:10.1016/j.jphotochem.2021.113129

Li, X., Zhang, S., Kulinich, S. A., Liu, Y., and Zeng, H. (2014). Engineering surface states of carbon dots to achieve controllable luminescence for solid-luminescent composites and sensitive Be2+ detection. *Sci. Rep.* 4, 4976–4978. doi:10.1038/srep04976

Liu, C., Zhang, F., Hu, J., Gao, W., and Zhang, M. (2021a). A mini review on pH-sensitive photoluminescence in carbon nanodots. *Front. Chem.* 8, 1–9. doi:10.3389/fchem.2020.605028

Liu, X., Xu, H., Zhang, M., and Yu, D. G. (2021b). Electrospun medicated nanofibers for wound healing: review. *Membranes* 11 (10), 770. doi:10.3390/membranes11100770

Lu, S., Li, Z., Fu, X., Xie, Z., and Zheng, M. (2021). Carbon dots-based fluorescence and UV–vis absorption dual-modal sensors for Ag+ and L-cysteine detection. *Dyes Pigments* 187, 109126. doi:10.1016/j.dyepig.2020.109126

Lucas, M., Freitas, M., Xavier, J. A., Moura, F. A., Goulart, M. O. F., Ribeiro, D., et al. (2021). The scavenging effect of curcumin, piperine and their combination against physiological relevant reactive pro-oxidant species using *in vitro* non-cellular and cellular models. *Chem. Pap.* 75 (10), 5269–5277. doi:10.1007/s11696-021-01710-y

Macairan, J. R., Zhang, I., Clermont-Paquette, A., Naccache, R., and Maysinger, D. (2020). Ratiometric pH sensing in living cells using carbon dots. *Part. Part. Syst. Charact.* 37 (1), 1–7. doi:10.1002/ppsc.201900430

Mary, S. K., Koshy, R. R., Arunima, R., Thomas, S., and Pothen, L. A. (2022). A review of recent advances in starch-based materials: bionanocomposites, pH sensitive films, aerogels and carbon dots. *Carbohydr. Polym. Technol. Appl.* 3, 100190. doi:10.1016/j.carpta.2022.100190

Mei, H., Gu, X., Wang, M., Chen, J., Yang, X., Liu, X., et al. (2022). A tri-response colorimetric-fluorescent probe for pH and lysosomal imaging. *Sensors Actuators B Chem.* 370, 132425. doi:10.1016/j.snb.2022.132425

Moghaddam, M. A., Martino, A. D., and Šopík, T. (2021). Polylactide/polyvinylalcohol-based porous bioscaffold loaded with gentamicin for wound dressing applications. *Polymers* 13 (6), 7–9. doi:10.3390/polym13060921

Moniruzzaman, M., Dutta, S. D., Lim, K. T., and Kim, J. (2022). Perylene-derived hydrophilic carbon dots with polychromatic emissions as superior bioimaging and NIR-responsive photothermal bactericidal agent. *ACS Omega* 7 (42), 37388–37400. doi:10.1021/acsomega.2c04130

Mosmann, T. (1983). Rapid colorimetric assay for cellular growth and survival: application to proliferation and cytotoxicity assays. *J. Immunol. Methods* 65, 55–63. doi:10.1016/0022-1759(83)90303-4

Naeem, F., Khan, S., Jalil, A., Ranjha, N. M., Riaz, A., Haider, M. S., et al. (2017). pH responsive cross-linked polymeric matrices based on natural polymers: effect of process variables on swelling characterization and drug delivery Properties. *Bioimpacts* 7 (3), 177–192. doi:10.15171/bi.2017.21

Nascimento, S. M. S. D., Sonsin, A. F., Barbosa, C. D. A., and Fonseca, E. J. S. (2023). Study of the pH effect on the optical and morphological properties of S, N self-doped carbon dots applied as fluorescent anti-counterfeiting ink and pH sensor. *Nanotechnology* 34 (36), 365708. doi:10.1088/1361-6528/acdc30

Omidi, M., Yadegari, A., and Tayebi, L. (2017). Wound dressing application of pH-sensitive carbon dots/chitosan hydrogel. *RSC Adv.* 7 (18), 10638–10649. doi:10.1039/c6ra25340g

Pandey, A. K., Bankoti, K., Nath, T. K., and Dhara, S. (2022). Hydrothermal synthesis of PVP-passivated clove bud-derived carbon dots for antioxidant, catalysis, and cellular imaging applications. *Colloids Surfaces B Biointerfaces* 220, 112926. doi:10.1016/j.colsurfb.2022.112926

Pang, Q., Yang, F., Jiang, Z., Wu, K., Hou, R., and Zhu, Y. (2023). Smart wound dressing for advanced wound management: real-time monitoring and on-demand treatment. *Mater. Des.* 229, 111917. doi:10.1016/j.matdes.2023.111917

Qu, X., Gao, C., Fu, L., Chu, Y., Wang, J. H., Qiu, H., et al. (2023). Positively charged carbon dots with antibacterial and antioxidant dual activities for promoting infected wound healing. *ACS Appl. Mater. Interfaces* 15 (15), 18608–18619. doi:10.1021/acsami.2c21839

Rodríguez-Varillas, S., Fontanil, T., Obaya, Á. J., Fernández-González, A., Murru, C., and Badía-Laíño, R. (2022). Biocompatibility and antioxidant capabilities of carbon dots obtained from tomato (Solanum lycopersicum). *Appl. Sci.* 12, 773. doi:10.3390/app12020773

Roy, S., Ezati, P., Rhim, J. W., and Molaei, R. (2022). Preparation of turmeric-derived sulfur-functionalized carbon dots: antibacterial and antioxidant activity. *J. Mater. Sci.* 57 (4), 2941–2952. doi:10.1007/s10853-021-06804-2

Sabzi, M., Afshari, M. J., Babaahmadi, M., and Shafagh, N. (2020). pH-dependent swelling and antibiotic release from citric acid crosslinked poly(vinyl alcohol) (PVA)/nano silver hydrogels. *Colloids Surfaces B Biointerfaces* 188, 110757. doi:10.1016/j.colsurfb.2019.110757

Sharma, S., Mohler, J., Mahajan, S. D., Schwartz, S. A., Bruggemann, L., and Aalinkeel, R. (2023). Microbial biofilm: a review on formation, infection, antibiotic resistance, control measures, and innovative treatment. *Microorganisms* 11 (6), 1614. doi:10.3390/microorganisms11061614

Sies, H., Berndt, C., and Jones, D. P. (2017). Oxidative stress. *Annu. Rev. Biochem.* 86, 715–748. doi:10.1146/annurev-biochem061516-045037

Singh, A., Qu, Z., Sharma, A., Singh, M., Tse, B., Ostrikov, K., et al. (2022). Ultra-bright green carbon dots with excitation-independent fluorescence for bioimaging. *J. Nanostructure Chem.* 13 (3), 377–387. doi:10.1007/s40097-022-00501-5

Smrithi, S. P., Kottam, N., Muktha, H., Mahule, A. M., Chamarti, K., Vismaya, V., et al. (2022). Carbon dots derived from Beta vulgaris: evaluation of its potential as antioxidant and anticancer agent. *Nanotechnology* 33 (4), 045403. doi:10.1088/1361-6528/ac30f1

Song, W., Duan, W., Liu, Y., Ye, Z., Chen, Y., Chen, H., et al. (2017). Ratiometric detection of intracellular lysine and pH with one-pot synthesized dual emissive carbon dots. *Anal. Chem.* 89 (24), 13626–13633. doi:10.1021/acs.analchem.7b04211

Suhail, M., Fang, C. W., Khan, A., Minhas, M. U., and Wu, P. C. (2021). Fabrication and *in vitro* evaluation of pH-sensitive polymeric hydrogels as controlled release carriers. *Gels* 7 (3), 110. doi:10.3390/gels7030110

Tadesse, A., Devi, D. R., and Hagos, M. (2018). Facile green synthesis of fluorescent carbon quantum dots from citrus lemon juice for live cell imaging. *Asian J. Nanosci. Mater.* 1 (1), 36–46. doi:10.26655/ajnanomat.2018.1.5

Tamayol, A., Akbari, M., Zilberman, Y., Comotto, M., Lesha, E., Serex, L., et al. (2016). Flexible pH-sensing hydrogel fibers for epidermal applications. *Adv. Healthc. Mater.* 5 (6), 711–719. doi:10.1002/adhm.201500553

Tang, N., Zheng, Y., Jiang, X., Zhou, C., Jin, H., Jin, K., et al. (2021). Wearable sensors and systems for wound healing-related ph and temperature detection. *Micromachines* 12 (4), 430–515. doi:10.3390/mi12040430

Taspika, M., Permatasari, F. A., Nuryadin, B. W., Mayangsari, T. R., Aimon, A. H., and Iskandar, F. (2019). Simultaneous ultraviolet and first near-infrared window absorption of luminescent carbon dots/PVA composite film. *RSC Adv.* 9 (13), 7375–7381. doi:10.1039/c8ra09742a

Venugopalan, P., and Vidya, N. (2023). Microwave-assisted green synthesis of carbon dots derived from wild lemon (Citrus pennivesiculata) leaves as a fluorescent probe for tetracycline sensing in water. *Spectrochimica Acta - Part A Mol. Biomol. Spectrosc.* 286, 122024. doi:10.1016/j.saa.2022.122024

Wang, B., Cai, H., Waterhouse, G. I. N., Qu, X., Yang, B., and Lu, S. (2022). Carbon dots in bioimaging, biosensing and therapeutics: a comprehensive review. *Small Sci.* 2 (6), 2200012. doi:10.1002/smsc.202200012

Wang, Z., Liu, L., Bu, W., Zheng, M., Jin, N., Zhang, K., et al. (2020). Carbon dots induce epithelial-mesenchymal transition for promoting cutaneous wound healing via activation of TGF-β/p38/snail pathway. *Adv. Funct. Mater.* 30 (43), 2004886. doi:10.1002/adfm.202004886

Wei, X. L., Shi, Q. L., Jiang, L., and Qin, Y. (2023). Multicolour carbon dots with excitation-independent emission by microwave solvothermal reaction. *Carbon Lett.* 33 (1), 191–201. doi:10.1007/s42823-022-00416-9

Wu, X., Abbas, K., Yang, Y., Li, Z., Tedesco, A. C., and Bi, H. (2022). Photodynamic anti-bacteria by carbon dots and their nano-composites. *Pharmaceuticals* 15 (4), 487–521. doi:10.3390/ph15040487

Xavier, J., Valentim, I. B., Camatari, F. O. S., de Almeida, A. M. M., Goulart, H. F., Ferro, J. N. S., et al. (2017). Polyphenol profile by uhplc-ms/ms, anti-glycation, antioxidant and cytotoxic activities of several samples of propolis from the northeastern semi-arid region of Brazil. *Pharm. Biol.* 55 (1), 1884–1893. doi:10.1080/13880209.2017.1340962

Xia, C., Cao, M., Xia, J., Zhou, G., Jiang, D., Zhang, D., et al. (2019). An ultrafast responsive and sensitive ratiometric fluorescent pH nanoprobe based on label-free dual-emission carbon dots. *J. Mater. Chem. C* 7 (9), 2563–2569. doi:10.1039/c8tc05693e

Xu, S., He, X., Huang, Y., Liu, X., Zhao, L., Wang, X., et al. (2020). Lysosome-targeted ratiometric fluorescent sensor for monitoring pH in living cells based on one-pot-synthesized carbon dots. *Microchim. Acta* 187 (8), 478–516. doi:10.1007/s00604-020-04462-w

Yang, P., Zhu, Z., Zhang, T., Zhang, W., Chen, W., Cao, Y., et al. (2019). Orange-emissive carbon quantum dots: toward application in wound pH monitoring based on colorimetric and fluorescent changing. *Small* 15 (44), 1–11. doi:10.1002/smll.201902823

Zafar, N., Mahmood, A., Ilyas, S., Ijaz, H., Muhammad Sarfraz, R., Mahdi, W. A., et al. (2023). Novel Natrosol/Pectin-co-poly acrylate based pH-responsive polymeric carrier system for controlled delivery of Tapentadol Hydrochloride. *Saudi Pharm. J.* 31 (8), 101671. doi:10.1016/j.jsps.2023.06.004

Zhang, T., Dong, S., Zhao, F., Deng, M., Fu, Y., and Lü, C. (2019). Tricolor emissive carbon dots for ultra-wide range pH test papers and bioimaging. *Sensors Actuators, B Chem.* 298, 126869. doi:10.1016/j.snb.2019.126869

Zhu, Y., Zhang, J., Song, J., Yang, J., Du, Z., Zhao, W., et al. (2020). A multifunctional pro-healing zwitterionic hydrogel for simultaneous optical monitoring of pH and glucose in diabetic wound treatment. *Adv. Funct. Mater.* 30 (6), 1–9. doi:10.1002/adfm.201905493